Pakistan Veterinary Journal

ISSN: 0253-8318 (PRINT), 2074-7764 (ONLINE)
DOI: 10.29261/pakvetj/2025.342

RESEARCH ARTICLE

# Clade Dynamics and Persistence of ALV-J in Taiwan Poultry Populations

Cheng-Hsun Wu1¶, Dai-Lun Shin[2¶], Yi-Wen Cheng[1], Wei-Hsiang Huang[3] and Nai-Huei Wu[1*]

[1]Department and Graduate Institute of Veterinary Medicine, National Taiwan University, Taiwan; [2]Department of Veterinary Medicine, National Chung Hsing University, Taiwan; [3]Graduate Institute of Molecular and Comparative Pathobiology, National Taiwan University, Taiwan. ¶equally contribution
*Corresponding author: naihueiwu@ntu.edu.tw

ARTICLE HISTORY (25-1083)

Received: November 09, 2025
Revised: December 14, 2025
Accepted: December 17, 2025
Published online: January 09, 2026

**Key words:**
Avian leukosis virus
Clade dynamics
Co-infection
DR-1 motif
Phylogenetic analysis
RCAS system

**ABSTRACT**

Avian leukosis virus subtype J (ALV-J) remains a persistent threat to the poultry industry. To address a decade-long data gap in Taiwan, we surveyed 41 colored-broiler or layer farms using field-submitted, tumor-suspect samples collected between 2021 and 2023. Eight ALV-J–positive cases were detected, including five clade 2 and three clade 1, no clade 3 cases were found. Three of the eight cases showed co-infection with ALV-K. Sequence analysis of gp85 from newly isolated ALV-J viruses, together with historical Taiwan isolates from 2000 to 2010, revealed a shift from HPRS-103-like (clade 1) to ADOL-7501-like (clade 2) viruses. Although multiple 3′UTR conformations were observed, the DR-1 element remained conserved. To assess the infectivity of current Taiwanese strains, we used the RCAS system to generate recombinant viruses harboring the clade 2 env and the DR-1 region, showing an enhancement of replication kinetics in DF-1 cells compared to env alone. Our results indicate that DR-1 promotes clade 2 replication, consistent with prior findings on clade 1. These data confirm the continued circulation of ALV-J in Taiwan, ongoing genomic evolution, and field co-infections of ALV-J and ALV-K. Our findings provide updated baseline information that can inform future monitoring and control strategies across Taiwan's diverse poultry production systems.

**To Cite This Article:** Wu CH, Shin DL, Cheng YW, Huang WH and Wu NH, 2025. Clade dynamics and persistence of alv-j in taiwan poultry populations. Pak Vet J. http://dx.doi.org/10.29261/pakvetj/2025.342

## INTRODUCTION

Avian leukosis virus (ALV) remains an important pathogen in commercial and native chickens, where infections lead to lymphoid and myeloid leukosis, production losses, glioma (Nishiura *et al.*, 2023), and immunosuppression (Borodin *et al.*, 2022). ALV belongs to the genus *Alpharetrovirus* in the family *Retroviridae*, the genome had been divided into segmental parts, LTR facilitates the integration of proviral DNA into the host genome, while the env gene encodes gp85 (surface, SU), which includes five variable regions (vr1, vr2, hr1, hr2, vr3) alongside gp37 (transmembrane, TM) proteins, determining host range and subtype via receptor binding (Dorner and Coffin, 1986; Federspiel, 2019). ALV is categorized into eleven subgroups (A–K) based on gp85 sequence, host range, and interference patterns. Subgroups A–D, J, and K are exogenous, whereas the others are endogenous and are distinguished by interference assays rather than cross-reactive neutralization (Payne and Nair, 2012). The ALV-J subtype was first identified in British broilers in 1988. Later, the HPRS-103-like viruses were detected globally, including in Asia and the Middle East (Payne and Nair, 2012). Early clade 1 ALV-J (prototype HPRS-103) often caused lifelong viremia/shedding, unlike other subtypes (Fadly and Smith, 1999). Around the year 2000, the ALV-J virus had evolved and adapted to layer, which could be represented by ADOL-7501, causing hemangiomas after infection. In Taiwan, the first reports of ALV involvement could be traced back to an outbreak of myeloid leukemia in chickens in 1995, resulting in high mortality rates (Wang *et al.*, 1995). Later reports showed that the severe situation occurred at a grandparent breeder farm, which suffered economic losses due to an ALV-J outbreak in 1997 (Wang and Juan, 2002). The emerging subtype ALV-K was classified from Chinese Luhua chickens (JS11C1) in 2012 (Li *et al.*, 2016). The first ALV-K subtype isolate in Taiwan (TW-3593) was initially classified as "ALV-A-like J virus" in 2010, exhibiting a high prevalence in Taiwanese native chicken farms (Chang *et al.*, 2013).

The 3' untranslated region (3' UTR) behind the env gene contains cis-regulatory elements (CREs), such as r-TM, which has been linked to pathogenicity in laying hens (Wang *et al.*, 2012), and DR-1 (direct repeat 1), which promotes

viral mRNA exportation (Ogert *et al.*, 1996). The XSR (E element) has been found not to be directly correlated with viral tumorigenesis, but rather highly associated with the pathogenicity of ALV-J (Chesters *et al.*, 2006).

Since ALV viruses can cause acute oncogenesis by integrating proviral DNA into the host genome, retrovirus vectors based on ALV have been developed. The functional Replication-Competent ALV LTR with a Splice Acceptor (RCAS) vector has been established from the Rous sarcoma virus SR-A strain, which can be used to rescue recombinant viruses in avian cell lines or transiently express target genes (Hughes, 2004). To date, RCAS has been widely used in embryology, gene therapy, and ALV studies (Gordon *et al.*, 2009). For instance, the determination of ALV pathogenicity in lymphoid or myeloid leukosis had been studied (Chesters *et al.*, 2002).

This study investigates ALV-J infections in Taiwan from 2021 to 2023 and characterizes isolates through gp85 phylogeny and histopathological analysis. It addresses a decade-long gap in the ALV surveillance in Taiwan. The replication machinery of the DR-1 region of ALV-J clade 2 in terms of viral replication was studied by using the RCAS system.

## MATERIALS AND METHODS

**Case Collection:** Tumor-suspected samples were collected via passive-field submission between 2021 and 2023 from layer and indigenous chicken farms across Taiwan. A total of 41 Taiwanese poultry farms showing weakness, loss of egg production, growth retardation, or enlarged livers or spleens in chickens were identified. All the specimens were fixed in 10% formalin for histopathologic examination. Tissue homogenates (~1 cm² in 1:10 DMEM + 1% P/S) were centrifuged (1,500 rpm, 8 min); supernatant was used for nucleic acid extraction and virus isolation. Blood was diluted 1:1 with PBS, layered over 3 mL Ficoll-Paque PLUS, centrifuged (400×g, 20°C, 30 min), and plasma/PBMCs stored at -80°C.

**Histological Evaluation and Immunohistochemistry:** For histology and immunohistochemistry, organs were collected and fixed by immersion in 10% buffered formalin. Tissues were embedded in paraffin and cut into 3 µm-thick sections. Histopathology was evaluated on haematoxylin and eosin (HE) stained sections in a blinded fashion. All tissue sections were digitized using a 3DHISTECH Pannoramic MIDI II digital whole-slide scanner. The scanned images were subsequently archived and evaluated for further analysis.

For the detection of avian leukosis virus antigen and immune cells, immunohistochemistry was performed as described previously (Yang *et al.*, 2025). The following antibodies were used: home-made mouse anti-ALV-J monoclonal antibody mAb22 (1:1 with hybridoma conditioned medium, kindly provided by Prof. Ching-Ho Wang), CD3 (T cells, Agilent Technologies, clone F7.2.38, 1:100), and Pax5 (B cells, Leica Biosystems, NCL-L-PAX-5, 1:100). Primary antibodies were applied for 1 hour at room temperature. Detection was performed either using the Dako EnVision+ polymer system (Dako Agilent Pathology Solutions).

**Virus isolation, nucleic acid detection, and sequence analysis:** Nucleic acids were extracted from organ homogenates, plasma, and PBMCs. DNA was extracted using the QIAamp DNA Mini Kit (Qiagen, Germany), and RNA was extracted using the E.Z.N.A.® Tissue RNA Kit (Omega Bio-tek, USA), following the manufacturer's instructions. RNA was reverse transcribed into cDNA using random hexamer primers and M-MLV RTase (Invitrogen, USA). ALV-A/J/K was detected by RT-PCR (env primers, Table 1); MDV/REV was detected by PCR. Reactions used Taq 2x Master Mix RED in Bio-Rad C1000. Positives were visualized on 1.5% agarose gels and confirmed by sequencing.

**Table 1:** Primer used in the study

| Name | Sequence（5'->3'） | Polarity | Location | Reference |
|---|---|---|---|---|
| Diagnosis primers | | | | |
| *ALV-A* | | | | |
| PA1 | CTACAGCTGTTAGGTTCCCAGT | sense | 5786-5807 | (Chang *et al.*, 2013) |
| TWA | ACYSGRTTTCAGGAAGRCCC | antisense | 6128-6109 | |
| *ALV-K* | | | | |
| P1 | TCCAGGCCGCAACTCAC | sense | 5853-5869 | (Chen *et al.*, 2018) |
| P2 | CATACCACCACCCACGTACT | antisense | 7066-7047 | |
| *ALV-J* | | | | |
| H5 | GGATGAGGTGACTAAGAAAG | sense | 5258-5277 | (Smith *et al.*, 1998) |
| H7 | CGAACCAAAGGTAACACACG | antisense | 5802-5783 | |
| *MDV* | | | | |
| MR-S | TGTTCGGGATCCTCGGTAAGA | sense | | (Murata *et al.*, 2007) |
| MR-AS | AGTTGGCTTGTCATGAGCCAG | antisense | | |
| *REV* | | | | |
| REV-F | CATACTGGAGCCAATGGTT | sense | | (Rong, 2001) |
| REV-R | AATGTTGTAGCGAAGTACT | antisense | | |
| RCAS cloning primers | | | | |
| mixA | TAAGGCAGTACATGGGTGGTG | sense | | |
| mixB | CTTTCTTAGTCACCTCATCCTTTTG | antisense | | |
| mixD | CACCACCCATGTACTGCCTTACAGCTGCTCCCTAATTCTATG | antisense | | |
| RCAS-JE-UF | CCCAAATAACCTTATCAGTGTCC | antisense | | This study |
| JE-UF | GACACTGATAAGGTTATTTGGGT | sense | | |
| DR-cut-mix | CACCACCCATGTACTGCCTTATG TTCTGAGGGGATTCCTAT | antisense | | |

PBMCs/tissues homogenized were inoculated onto DF-1 cells (5.6 × $10^5$/T25) in DMEM. After 4 hours of inoculation, the medium was changed to 2% FBS, followed by 5% every 3 days. Third-passage supernatants were subjected to RT-PCR testing for ALV subtype-specific confirmation. Positive supernatants were sequenced, aliquoted, and stored at -80°C for further analysis.

The *env* gene was sequenced either by assembling overlapping fragments amplified with specific primers (Table 1) or by TA cloning into the pCR™2.1-TOPO vector (Invitrogen, USA). Sanger sequencing results were compiled using BioEdit version 7.2.5. Align with reference sequences (NCBI database) by using the ClustalW method in MEGA 11. Phylogenetic trees were constructed with the neighbor-joining method using 1,000 bootstrap replicates.

**RCAS(J) 21-01 plasmid and virus construction:** A subgroup J reporter virus, RCAS(J) 21-01-EGFP, was constructed using the local Av21-01 strain. The RCAS(A)-EGFP backbone (provided by Dr. Stephen H. Hughes) was propagated in DH5α ECOS-101 cells and sequence-verified. The envelope was replaced with Av21-01 env, in two variants: with or without the DR-1 region. For env-only, primer pair mixA/mixB amplified the vector and H5/mixD the insert; for env+DR1, mixA/RCAS-JE-UF and JE-UF/DR-cut-mix were used (primers in Table 1). Gibson assembly (NEBuilder® HiFi, 50°C, 90 min) joined fragments, followed by transformation into ECOS-101, plating on LB-ampicillin, and colony PCR screening. Positive plasmids were purified using QIAprep Spin Miniprep Kit (Qiagen). For virus generation, confluent DF-1 cells were electroporated with 20 µg plasmid (200 V, 40 ms) in Opti-MEM™, recovered on ice, and plated in DMEM/2% FBS. The medium was switched to 5% FBS after 24 hours. Cells were monitored via fluorescence microscopy (Zeiss Axio Observer 7); upon strong GFP and confluence, they were passaged. Supernatants were harvested, filtered (0.45 µm), and stored at -80°C. GFP-positive area per passage was quantified in five random fields using ImageJ (8-bit, threshold 50–255). The percentage of GFP-positive area in DF-1 monolayers serves as the primary parameter to assess viral replication and spread kinetics (Matoušková *et al.*, 2024).

## RESULTS

**Tumor case detection and histopathology:** Tumor-suspected cases were passively submitted between 2021 and 2023 from layer and indigenous chicken farms distributed across northern, central, and southern Taiwan (41 farms in total), with most submissions originating from central and southern regions. Flock size and geo-location information for ALV-positive farms were available and are summarized in Table 2. A notable case from Yunlin County was introduced (Av21-01). The farm bred 3,000 colored chickens, which showed emaciation, gasping, and a daily mortality rate of 1–10 birds from 18 weeks of age. Morbidity reached 10% (300/3,000), and mortality was 4% (120/3,000) in 26-week-old and submitted for pathological diagnosis. Gross pathology revealed pale chest muscles, enlarged liver with multifocal white nodules and hemorrhage granules (indicative of tumors, Fig. 1A), swollen kidneys with pale cortices, splenomegaly with mottled surfaces, adheres with a yellowish to pale soft mass in one examined chicken (Fig. 1B), hemorrhages in the digestive tract, and enlarged pancreas/duodenum with nodular infiltrates.

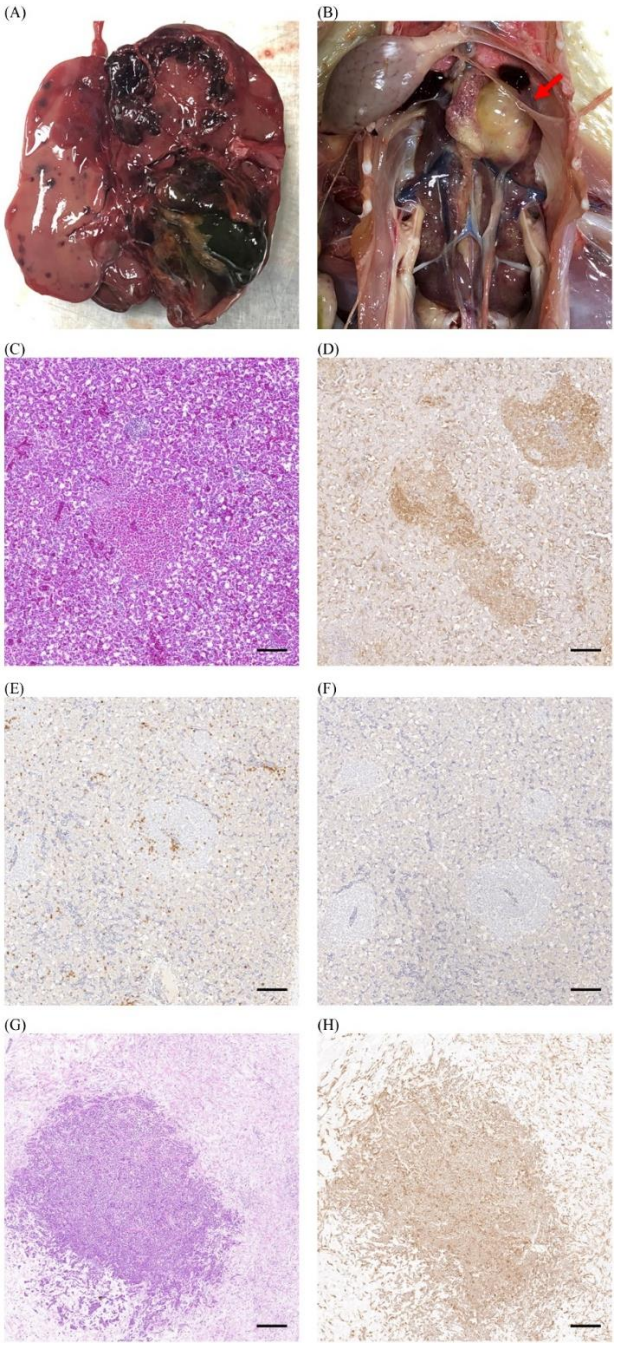


**Fig. 1:** Histopathological and immunohistochemical analysis of ALV-J infection in a 25–26-week-old colored broiler from Yunlin County, Taiwan (A) Gross pathology of enlarged liver with multifocal white nodules and hemorrhagic foci. (B) Gross pathology of abdominal cavity showing pale mass adhering to kidney (arrow). (C) Liver section (H&E, ×10) with multifocal to diffuse infiltration of neoplastic cells expanding portal areas and sinusoids. (D) Liver immunohistochemistry with mouse anti-ALV-J mAb22 showing cytoplasmic positivity in neoplastic cells. (E) Immunohistochemical staining of the liver with CD3, a small number of CD3-positive T cells infiltrated in the field without association with the tumor area. (F) Immunohistochemical staining of the liver with Pax5, showing negativity for B cells. (G) Histopathological section of the fibroma adhered to the kidney (H&E, ×5), exhibiting multifocal infiltration of eosinophilic myelocytes and proliferation of fibroblast-like cells. (H) Immunohistochemical staining of the kidney-adhered mass with mouse anti-ALV-J mAb22, extensive ALV-J-positive granulocytic cell infiltration. Scale bars = 100 µm (C-F), 200µm (G-H).

**Table 2:** Information on eight ALV-J positive farms and isolates in the study

| Case | Collecting date | Breed | Geolocation | Flock size | Age (week) | ALV-J Clade 1 | ALV-J Clade 2 | ALV-K |
|---|---|---|---|---|---|---|---|---|
| Av21-01 | 2021.Jul | Colored broilers | Yunlin county | 3000 | 26 | | + (isolated) (PX688644) | |
| Av22-13 | 2022.Dec | Layers | Changhua county | 9000 | 19 | | + | |
| Av23-03 | 2023.Jan | Layers | Changhua county | 18000 | 35 | + (isolated) (PX688645) | | |
| Av23-25 | 2023.May | Silky fowl | Chiayi county | 22000 | 20 | | + (isolated) (PX688646) | + (PX688651) |
| Av23-30 | 2023.May | Colored broilers | Yunlin county | 14000 | 8 | | + (isolated) (PX688647) | + (PX688650) |
| Av23-33 | 2023.May | Capon | Taitung county | 400 | 18 | + (isolated) (PX688648) | | + (PX688652) |
| Av23-36 | 2023.Jun | Colored broilers | Yunlin county | 14000 | 12 | | + (PX688649) | |
| Av23-41 | 2023.Aug | Layers | Taoyuan county | 20000 | 113 | + | | |

GenBank accession numbers for ALV-J and ALV-K env/3'UTR sequences are listed in parentheses (PX688644–PX688652).

Histopathological examination demonstrated multifocal to diffuse infiltration of uniform lymphoid cells in multiple organs. In the liver, neoplastic lymphocytes expanded portal areas and sinusoids, compressing hepatocytes (Fig. 1C). Kidneys exhibited interstitial lymphoid aggregates disrupting tubules, while the splenic parenchyma was effaced by sheets of neoplastic lymphoblasts. In the pale enlarged mass adhered to the kidney, histopathology determination of proliferation of fibroblast-like cells, along with massive infiltration of myelocytes, was observed in the center of the fibroma region. The pancreas and duodenum had perivascular lymphoid cuffs, and diffuse infiltration of myelocytes was observed. Digital scanned figures were blindly evaluated, confirming neoplastic proliferation, no significant necrosis or fibrosis within the determination area associated with ALV-induced tumor. Homemade mAb22 monoclonal antibody against ALV-J subtype showed strong immunoreactivity in the neoplastic area, and positive cells were massively infiltrated in the intestinal tract, liver (Fig. 1D), kidney, lung, ovary, and a mass adhering to the kidney (Fig. 1G-1H). Both CD3 and Pax5 were negative under the IHC microscopy diagnosis process (Fig. 1E-1F).

Samples (organ homogenates, plasma, PBMCs) were examined by PCR/RT-PCR methods. Data on breeds, ages, results, and isolation are in Table 2. Farms were positive as follows: ALV-J in 8/41 (19.51%), and ALV-K in 3/41 (7.32%). Co-infections had also been detected, including cases such as Av23-25 (ALV-J, ALV-K), Av23-30 (ALV-J, ALV-K), and Av23-33 (ALV-J, ALV-K). REV was not present. For the notable Yunlin case, all animals were ALV-J positive but negative for ALV-A, MDV, and REV.

**ALV Virus isolation:** Using the RT-PCR method described above with ALV-specific primer pairs, samples of organ homogenates or PBMCs that showed positive results were selected for virus isolation in DF-1 cells. Specimen homogenate was directly inoculated on top of sub-confluent DF-1 cells and blind passage at least three times. In each passage, the inoculum was further confirmed by RT-PCR using subgroup-specific primers (Table 1) to confirm the isolation.

Five ALV-J viruses were successfully isolated, without showing cytopathic effects on DF-1 cells. The viruses were named Av21-01, Av23-03, Av23-25(J), Av23-30(J), and Av23-33(J) based on their case numbers and subtypes. These viruses were later used for sequence analysis and processing biological characterization.

**Sequence analysis and comparison:** The *env* gene of ALV isolates was amplified using RT-PCR and cloned using the TOPO TA Cloning Kit (Invitrogen, USA). The env and 3′UTR sequences of ALV-J isolates (Av21-01, Av23-03, Av23-25J, Av23-30J, Av23-33J, Av23-36J) and ALV-K isolates (Av23-25K, Av23-30K, Av23-33K) have been deposited in GenBank under accession numbers PX688644–PX688652 (see Table 2). Sanger sequencing of the env was performed and was aligned with the sequence of reference strains (e.g., HPRS-103 prototype, Table 3) at both nucleotide and amino acid levels. The alignment results showed that ALV-J isolates (TW-3594(J), Av21-01, Av23-03, Av23-25(J), Av23-30(J), Av23-33(J)) showed significant variability before position 100 of the *env* protein, particularly in variable regions of gp85 (vr1, Fig. 2A). In residues 40 to 69 of the env, two patterns, Av21-01, Av23-25(J), and Av23-30(J), were clustered with TW-3594(J), while AV23-03 and AV23-33(J) belong to a different branch, which is closer to the GX15JL01 strain from China. Similarity analysis indicated Av21-01 and Av23-30(J) shared the highest identity (95.0% amino acid, 95.2% nucleotide) (Fig. 3). Additionally, 3'UTR nucleotide alignments for r-TM, DR-1 elements, together with XSR region of ALV-J (Fig. 4) had been analyzed.

**Table 3:** Reference strains used for sequence analysis in the study

| Strains | Subgroup | Host | Location | Time | GenBank Accession No. |
|---|---|---|---|---|---|
| HPRS103 | J | Broiler | UK | 1988 | Z46390 |
| MRL905 | J | Commercial | Russia | 2009 | JF951728 |
| GX15JL01 | J | Domestic | China | 2015 | MN735294.1 |
| GD1407 | J | yellow chicken | China | 2014 | KU500034 |
| GD1109 | J | commercial layer | China | 2011 | JX254901.1 |
| JS09GY2 | J | commercial layer | China | 2009 | GU982307 |
| PK19FA01 | J | desi chicken | Pakistan | 2018 | MN956379.1 |
| PK19SA01 | J | desi chicken | Pakistan | 2018 | MN956380.1 |
| SDAU1704 | J | commercial layer | China | 2017 | KY980660.1 |
| PDRC-59831 | J | Broiler | USA | 2007 | KP284572.1 |
| JL093-1 | J | commercial layer | China | 2009 | JN624878.1 |
| GD18HZ11 | J | unknown | China | 2018 | MN262609.1 |
| AF88 | J | broiler breeder | USA | 1997 | AF247390 |
| GDQJ-1 | J | Unknown | China | 2014 | KU254611 |
| SCSM00 | J | Unknown | China | 2010 | KF796652 |
| ADOL-7501 | J | Broiler | USA | 1997 | AY027920 |
| HB18XH01 | J | yellow chicken | China | 2018 | MN735298.1 |
| QL1 | J | Layer | Egypt | 2019 | MN496121.1 |
| GD17ZQ08 | J | unknown | China | 2017 | MN262606.1 |
| JX19DX14 | J | unknown | China | 2019 | MN262582.1 |
| TW99 | J | Broiler | Taiwan | 1997 | AF497905 |

**Generation of RCAS(J) 21-01-EGFP variants with and without the DR-1 region:** DF-1 cells transfected with RCAS(J) 21-01-EGFP variants (env-only and env+DR1) were monitored for EGFP expression using a Zeiss Axio Observer 7 fluorescence microscope (Fig. 5A-D). The env-only construct (RCAS(J) 21-01 env) displayed sparse EGFP signals by passage 3 (P3) and 7 (P7), with an average of 7.3–14.5% of cells exhibiting fluorescence (Fig. 5A-B). In contrast, the env+DR1 construct (RCAS(J) 21-01 env+DR1) exhibited robust EGFP expression following transfection at passage 0 (P0), with 60–70% of cells fluorescent by passage 3 (P3, Fig. 5C), increasing to over

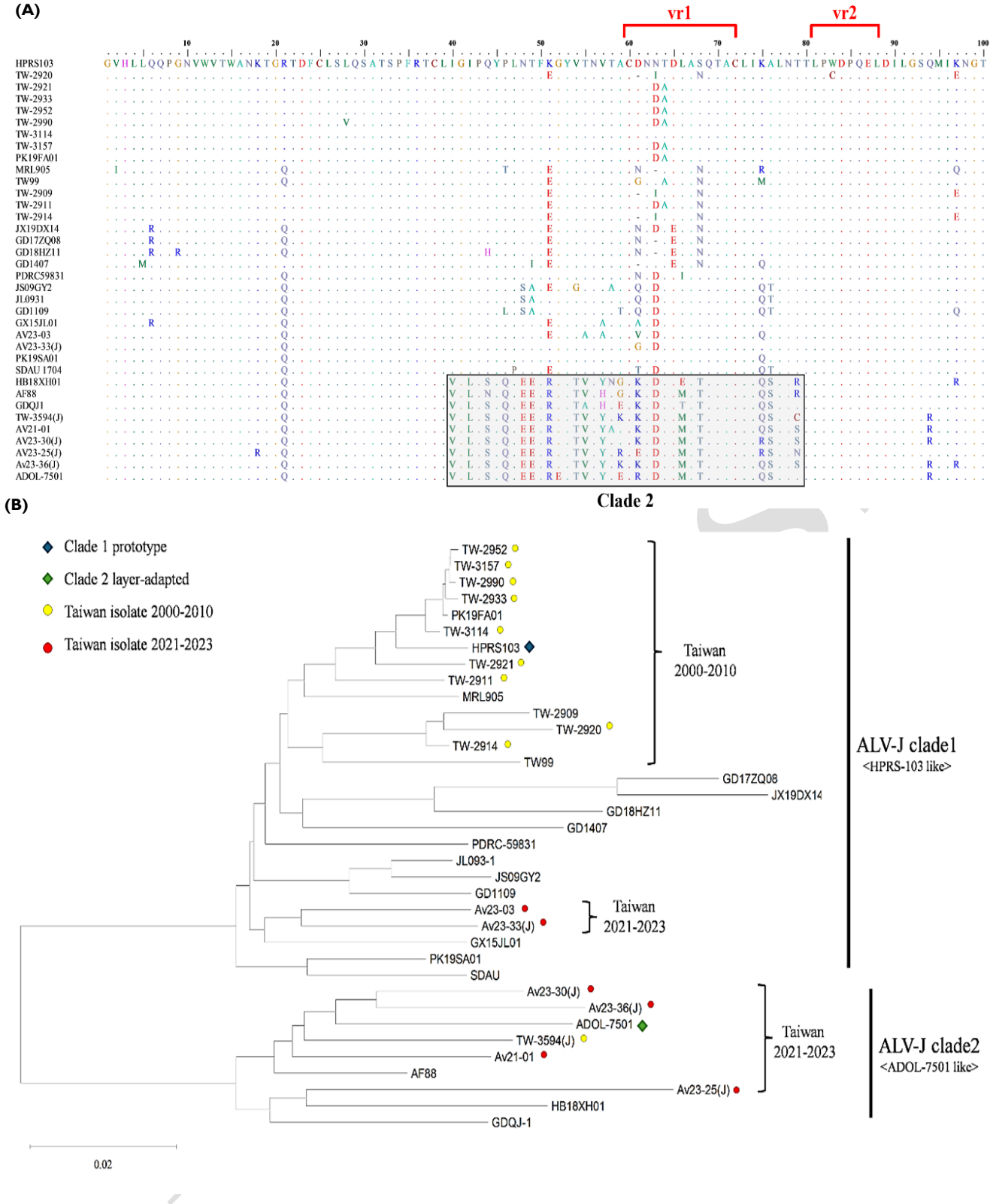


**Fig. 2:** Phylogenetic and Sequence Analysis of ALV-J env Gene Variants (A) Amino acid sequence alignment of the gp85 (SU) variable region 1 (vr1, residues 40–79) from Taiwanese isolates and reference strains. Grey box highlights the sequence variant region of vr1 in comparison between clade 1 and 2 ALV-J viruses. (B) Phylogenetic tree of gp85 nucleotide sequences. Taiwanese isolates from 2000 to 2010 (yellow circles) and isolates from 2021 to 2023 (red circles) are marked. Two clades represented by the HPRS-103 prototype (clade 1, blue diamond) and the layer-adapted ADOL-7501 (clade 2, green diamond) were marked, respectively. The scale bar represents 0.02 substitutions per site.

70% by passage 7 (P7) (Fig. 5D). ImageJ analysis of fluorescence images from five randomly selected fields per sample (technical replicates) revealed that env+DR1-infected cells exhibited a 6.2-fold higher fluorescent area (mean 62.9 ± 3.6% of total cell area) compared to env-only cells (mean 10.1 ± 2.3%) at passage 7 (P7; Fig. 5E). These data were obtained from seven to eight biological replicates across two independent experiments, and the difference between groups was significant in a two-tailed Mann–Whitney U test (p-value = 0.0003).

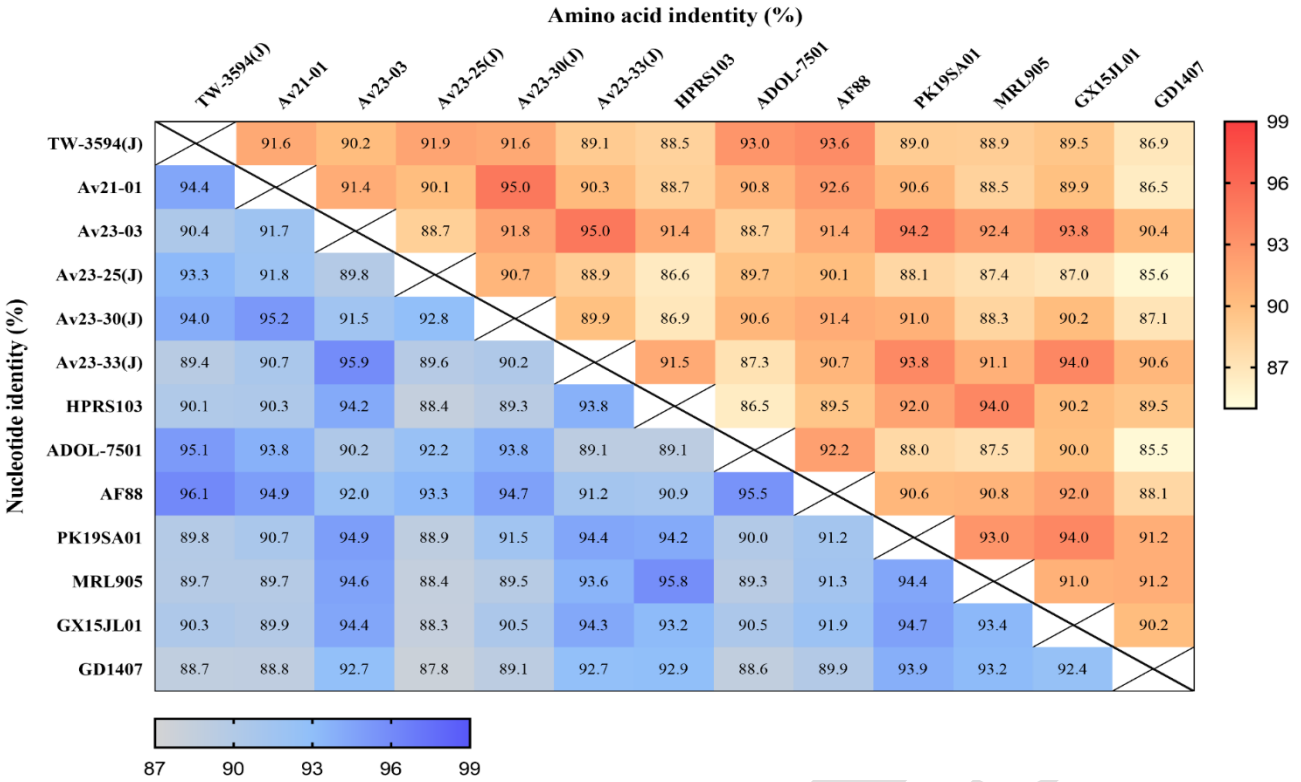


**Fig. 3:** Similarity matrix of ALV-J env nucleotide and amino acid sequences Pairwise identities were calculated using BioEdit. Orange cells represent amino acid similarity (85.5%-95.0%); blue cells represent nucleotide sequence similarity (87.8%-96.1%). Taiwanese Clade 1 (Av23-03, Av23-33J), and Clade 2 (Av21-01, Av23-25J, Av23-30J, TW-3594J) isolates aligned with HPRS-103 and ADOL-7501 reference strains, respectively.

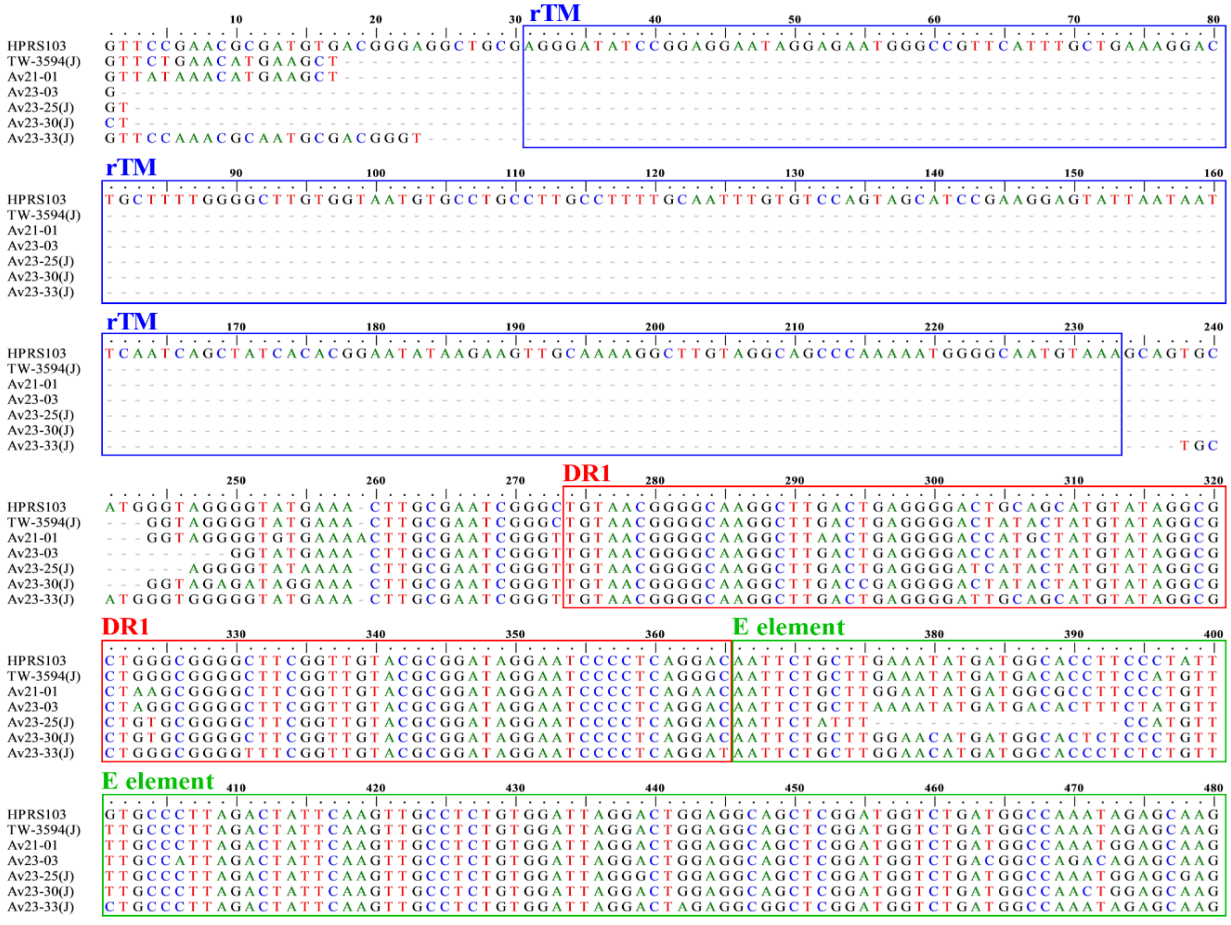


**Fig. 4:** Alignment of ALV-J 3′UTR nucleotide sequences from Taiwan isolates (2021–2023) The 3′UTR sequences of Clade 2 Taiwan isolates (TW-3594J, Av21-01, Av23-03, Av23-25J, Av23-30J, Av23-33J) were aligned with the Clade 1 prototype HPRS-103. Boxed regions indicate r-TM (blue), DR-1 (red), and XSR/E element (green), respectively. Dashes represent missing nucleotides in the corresponding strain.

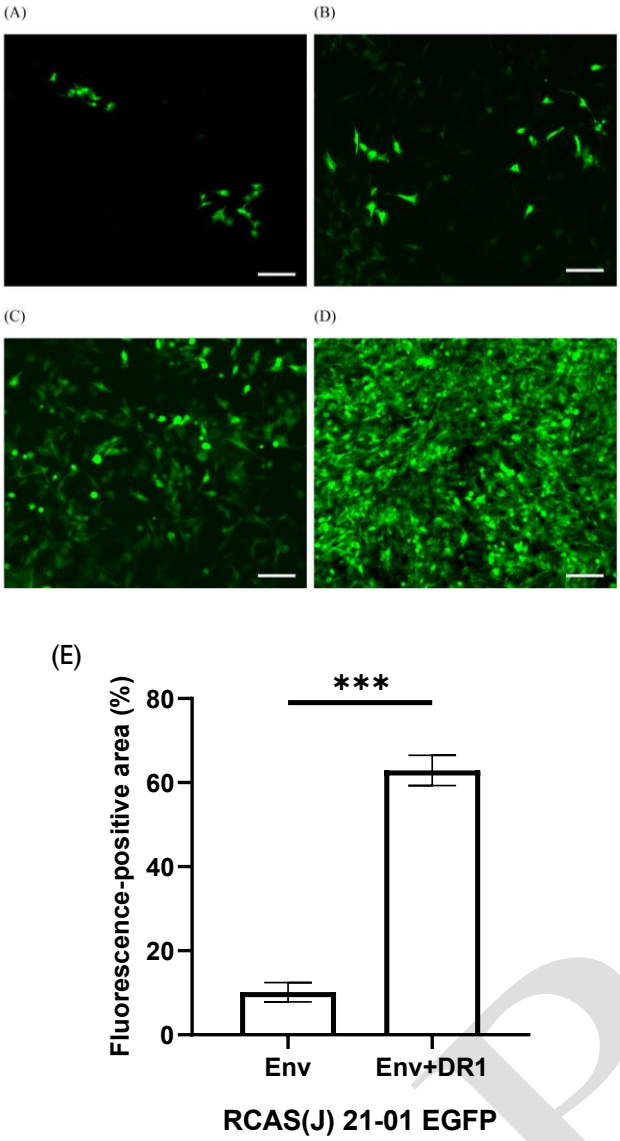


**Fig. 5:** Fluorescence microscopy images of DF-1 cells infected by RCAS(J) 21-01-EGFP variants (A–B) env-only construct (RCAS(J) 21-01 env) at passage 3 (P3) and 7 (P7), respectively. (C–D) env+DR1 construct (RCAS(J) 21-01 env+DR1) at P3 and P7. Scale bar: 100 μm. (E) Quantification of fluorescence-positive area at P7 (env n=7, env+DR1 n=8). Statistical analysis was performed using a two-tailed Mann–Whitney U test (***: p-value < 0.0001).

## DISCUSSION

**Current Status of ALV-J in Taiwan:** This study detected ALV in eight poultry cases out of forty-one farms collected between 2021 and 2023 in Taiwan, with ALV-J present in all eight cases and three cases positive for ALV-K. Thus, the suspected tumor cases in Taiwanese chicken farms are still predominantly ALV-J. In the Yunlin case, strong immunoreactivity of homemade mAb22 against ALV-J was detected in granulocytic neoplastic cells across multiple organs, confirming ALV-J as the etiological agent. The lack of CD3 and Pax5 staining indicated that infiltrates were neither T- nor B-cell lineage.

ALV-J is classified into three clades: Clade 1 (worldwide, oncogenic), Clade 2 (US, Egypt, China; layer-associated) (Deng *et al.*, 2022; Mo *et al.*, 2022; Payne and Nair, 2012), and Clade 3 (Chinese yellow chickens, associated with clade 1.3) distributed in the southern part of China (Deng *et al.*, 2021; Deng *et al.*, 2022). Phylogenetic analysis showed ALV-J isolates clustered into two major groups: Clade 1 (represented by HPRS-103) and Clade 2 (represented by ADOL-7501; Fig. 2B). Taiwan gp85 sequences from 2000–2010 (TW-2909~3157) fell in Clade 1, while four recent isolates (Av21-01, Av23-25J, Av23-30J, Av23-36J) belonged to Clade 2, similar to TW-3594J from 2010. Our newly isolated clade 1 strains Av23-03, Av23-33(J) formed a subgroup with the Chinese virus strain GX15JL01, while Clade 2 strains (Av21-01, Av23-25J, Av23-30J) closely matched ADOL-7501, AF88, and TW-3594J. Recent isolates show increased Clade 2 prevalence compared to historical Clade 1 dominance. Clade 3 viruses were hypothesize by inter-regional transport of poultry emerging in southern China. However, there is no direct animal contact or transmission between Taiwan and mainland China; no clade 3 was detected in Taiwan.

In our study, three cases were co-infected with ALV-J, corresponding to the global trend of 0–0.59% (Zhang *et al.*, 2024). The clinical signs were hepatosplenomegaly and poor uniformity in the flocks, which could not be solely attributed to ALV-K (Liang *et al.*, 2019). Co-infection with ALV-J exacerbates immunosuppression and neoplasia, which may be due to the synergistic effects of utilization of TvA and chNHE1 viral receptors (Matoušková *et al.*, 2024).

**Clade 2 ALV-J and layer adaptation:** The worldwide distribution of Clade 2 J viruses, such as ADOL-7501 and AF88, shows an enrichment in layer flocks in the US and China, with a documented post-2004 shift from broiler-associated intact r-TM with missing E, to a trend of E retention with r-TM loss pattern in laying hen outbreaks (Payne and Nair, 2012; Gao et al., 2012; Xu et al., 2023). However, in the dataset from Taiwan, Clade 2 was detected in both layers and colored broilers/specialty breeds, with no clear layer-specific enrichment. This differs from global patterns, likely due to: (1) diverse poultry production in Taiwan (longer-lived colored broilers alongside layers; (Thu and Wang, 2003); (2) passive tumor-suspect sampling bias toward clinically affected farms regardless of breed; and (3) limited sample size precluding statistical layer-broiler comparisons.

**DR-1 and 3'UTR function in virus spreading:** Functional studies in Clade 1 viruses have shown that deletion of the r-TM region enhances viral pathogenicity (Wang *et al.*, 2012), whereas loss of the E element promotes virus transcription and contributes to the broad adaptability of ALV-J across different chicken breeds. The DR-1 segment is an essential factor for mRNA nuclear export (Ogert *et al.*, 1996), and its consistent retention has been proposed to confer a selective advantage, facilitating host range expansion in both classical Clade 1 and post-2004 layer-associated strains (Gao *et al.*, 2012). In our 3'UTR sequence alignments, depletion of r-TM was observed in all newly characterized isolates, while variation in the E element was detected (Fig. 4). Interestingly, Av23-25(J) exhibited a 19-nucleotide deletion in E, similar to the emerging pattern with combined r-TM and E loss (Xu *et al.*, 2023). In contrast, the DR-1 element was conserved in all strains, prompting functional analysis of the Clade 2-derived DR-1.

Using the RCAS-EGFP system, we confirmed that DR-1 contributes to replication of a contemporary Taiwanese Clade 2 ALV-J strain. When env in RCAS(A)-EGFP was replaced with Av21-01 (J, Clade 2), env-only constructs induced only weak EGFP expression in DF-1 cells, whereas env+DR-1 variants showed robust EGFP expression from the first passage onward. This observation is in line with previous work on the Clade 1 strain HPRS-103, in which inclusion of DR-1 increased virus titers from approximately $10^2$ to $10^6$ $TCID_{50}$/mL (Chesters *et al.*, 2002; Kucerova *et al.*, 2013; Reinišová *et al.*, 2016). Including DR-1 from ALV-J, regardless of whether clade 1 or 2 is linked to enhanced replication, enabling them to persist in a wide variety of hosts. Further RCAS-based analysis of 3'UTR diversity, including different DR-1 and E-element configurations, should help to define more precisely how these motifs influence viral fitness and may provide useful information for future poultry control strategies.

**Conclusions:** This study provides an updated overview of ALV-J in Taiwan, following a decade-long gap in surveillance via integrating recent field data with historical information on viral evolution. The detection of ALV-J showed an apparent increase of Clade 2 and co-infections with ALV-K, further underscoring that the spectrum of retroviral infections in Taiwanese poultry has become more complex. Whereas the replication of Clade 2 virus consists of intact DR-1 and env gene compensation. Our findings provide relevant baseline information for further monitoring and control programs in the diverse poultry production systems of Taiwan.

**Acknowledgments:** Funding: This work was supported by the National Science and Technology Council (NSTC) [NSTC 112-2313-B-002-041-MY3, NSTC 113-2313-B-005-004-MY3]; the National Taiwan University within the framework of the Higher Education Sprout Project by the Ministry of Education (MOE) in Taiwan [NTU-113L7804, NTU-114L7864].

**Author Contributions:** Conceptualization, DLS, and NHW; Formal analysis, DLS, and NHW; Investigation, CHW, DLS, WHH, YWC, and NHW; Methodology: DLS, WHH and NHW; Resources, DLS and NHW; Writing – Original Draft, CHW, DLS, and NHW; Writing – Review & Editing, all authors; Funding acquisition, DLS and NHW.

We thank Prof. Ching-Ho Wang (National Taiwan University, Taiwan) for providing the monoclonal antibody and 2000–2010 Taiwan isolate sequence data, and Dr. Stephen H. Hughes (National Cancer Institute, NIH, United States) for the RCAS vector system.

**Disclosures:** The authors declare no conflict of interest in the present study.

## REFERENCES

Borodin AM, Emanuilova ZV, Smolov SV, *et al.*, 2022. Eradication of avian leukosis virus subgroups J and K in broiler cross chickens by selection against infected birds using multilocus PCR. PLoS One 17: e0269525.

Chang SW, Hsu MF, and Wang CH, 2013. Gene detection, virus isolation, and sequence analysis of avian leukosis viruses in Taiwan country chickens. Avian Dis 57: 172-7.

Chen J, Zhao Z, Chen Y, *et al.*, 2018. Development and application of a SYBR green real-time PCR for detection of the emerging avian leukosis virus subgroup K. Poult Sci 97: 2568-74.

Chesters PM, Howes K, Petherbridge L, *et al.*, 2002. The viral envelope is a major determinant for the induction of lymphoid and myeloid tumours by avian leukosis virus subgroups A and J, respectively. J Gen Virol 83: 2553-61.

Chesters PM, Smith LP, and Nair V, 2006. E (XSR) element contributes to the oncogenicity of Avian leukosis virus (subgroup J). J Gen Virol 87: 2685-92.

Deng Q, Li M, He C, *et al.*, 2021. Genetic diversity of avian leukosis virus subgroup J (ALV-J): toward a unified phylogenetic classification and nomenclature system. Virus Evol 7: veab037.

Deng Q, Li Q, Li M, *et al.*, 2022. The Emergence, Diversification, and Transmission of Subgroup J Avian Leukosis Virus Reveals that the Live Chicken Trade Plays a Critical Role in the Adaption and Endemicity of Viruses to the Yellow-Chickens. J Virol 96: e0071722.

Dorner AJ, and Coffin JM, 1986. Determinants for receptor interaction and cell killing on the avian retrovirus glycoprotein gp85. Cell 45: 365-74.

Fadly AM, and Smith EJ, 1999. Isolation and some characteristics of a subgroup J-like avian leukosis virus associated with myeloid leukosis in meat-type chickens in the United States. Avian Dis 43: 391-400.

Federspiel MJ, 2019. Reverse Engineering Provides Insights on the Evolution of Subgroups A to E Avian Sarcoma and Leukosis Virus Receptor Specificity. Viruses 11.

Gao Y, Yun B, Qin L, *et al.*, 2012. Molecular epidemiology of avian leukosis virus subgroup J in layer flocks in China. J Clin Microbiol 50: 953-60.

Gordon CT, Rodda FA, and Farlie PG, 2009. The RCAS retroviral expression system in the study of skeletal development. Dev Dyn 238: 797-811.

Hughes SH, 2004. The RCAS vector system. Folia Biol (Praha) 50: 107-19.

Kucerova D, Plachy J, Reinisova M, *et al.*, 2013. Nonconserved tryptophan 38 of the cell surface receptor for subgroup J avian leukosis virus discriminates sensitive from resistant avian species. J Virol 87: 8399-407.

Li X, Lin W, Chang S, *et al.*, 2016. Isolation, identification and evolution analysis of a novel subgroup of avian leukosis virus isolated from a local Chinese yellow broiler in South China. Arch Virol 161: 2717-25.

Liang X, Gu Y, Chen X, *et al.*, 2019. Identification and characterization of a novel natural recombinant avian leucosis virus from Chinese indigenous chicken flock. Virus Genes 55: 726-33.

Matoušková M, Plachý J, Kučerová D, *et al.*, 2024. Rapid adaptive evolution of avian leukosis virus subgroup J in response to biotechnologically induced host resistance. PLoS Pathog 20: e1012468.

Mo G, Wei P, Hu B, *et al.*, 2022. Advances on genetic and genomic studies of ALV resistance. J Anim Sci Biotechnol 13: 123.

Murata S, Chang KS, Lee SI, *et al.*, 2007. Development of a nested polymerase chain reaction method to detect oncogenic Marek's disease virus from feather tips. J Vet Diagn Invest 19: 471-8.

Nishiura H, Nakajima T, Saito S, *et al.*, 2023. Assessing avian leukosis virus proviral load and lesion correlates in fowl glioma-inducing virus-infected Japanese bantam chickens. J Vet Diagn Invest 35: 484-91.

Ogert RA, Lee LH, and Beemon KL, 1996. Avian retroviral RNA element promotes unspliced RNA accumulation in the cytoplasm. J Virol 70: 3834-43.

Payne LN, and Nair V, 2012. The long view: 40 years of avian leukosis research. Avian Pathol 41: 11-9.

Reinišová M, Plachý J, Kučerová D, *et al.*, 2016. Genetic Diversity of NHE1, Receptor for Subgroup J Avian Leukosis Virus, in Domestic Chicken and Wild Anseriform Species. PloS one 11(3), e0150589.

Rong J, 2001. Co-infection Detection of the Chicken Infectious Anemia Virus and Reticuloendotheliosis Virus in the Immunodepression Flock. Chinese Journal of Veterinary Drug.

Smith EJ, Williams SM, and Fadly AM, 1998. Detection of avian leukosis virus subgroup J using the polymerase chain reaction. Avian Dis 42: 375-80.

Thu WL, and Wang CH, 2003. Phylogenetic analysis of subgroup J avian leucosis virus from broiler and native chickens in Taiwan during 2000-2002. J Vet Med Sci 65: 325-8.

Wang CH, and Juan YW, 2002. Occurrence of subgroup J avian leukosis virus in Taiwan. Avian Pathol 31: 435-9.

Wang CH, Liu CF, Liu YF, *et al.*, 1995. High mortality in broiler flock with myelocytomatosis. J Chin Soc Vet Sci 21: 128-133.

Wang Q, Gao Y, Wang Y, *et al.*, 2012. A 205-nucleotide deletion in the 3' untranslated region of avian leukosis virus subgroup J, currently

emergent in China, contributes to its pathogenicity. J Virol 86: 12849-60.

Xu M, Qian K, Shao H, *et al*., 2023. 3'UTR of ALV-J can affect viral replication through promoting transcription and mRNA nuclear export. J Virol 97: e0115223.

Yang FH, Chang YP, Chang YC, *et al*., 2025. Insulinoma-associated protein 1 (INSM1) immunohistochemical expression in normal, hyperplastic, and neoplastic canine neuroendocrine tissues. Vet Pathol 62: 178-86.

Zhang F, Li H, Lin C, *et al*., 2024. Detection and genetic diversity of subgroup K avian leukosis virus in local chicken breeds in Jiangxi from 2021 to 2023. Front Microbiol 15: 1341201.